ORIENTAL JOURNAL OF CHEMISTRY
An International Open Access, Peer Reviewed Research Journal
www.orientjchem.org
ISSN: 0970-020 X
CODEN: OJCHEG
2025, Vol. 41, No.(2):
Pg. 409-417

Biosynthesis of Zinc Oxide Nanoparticles and Their Cytotoxicity Study on Fibroblast Cell Line Using MTT Assay

SHRAVANI RAMESH WADEKAR[1]*, MANISH SHAMRAO HATE[1] and RAMESH CHAUGHULE[2]

[1]*Research student, Ramnarain Ruia Autonomous College, L. N. Road, Matunga (east), Mumbai- 400019, India.
[1]Head of the Chemistry Department, Ramnarain Ruia Autonomous College, L.N. Road, Matunga (East), Mumbai-400019, India.
[2]Ex. Tata Institute of Fundamental Research, Mumbai, India Adjunct Professor, Ramnarain Ruia Autonomous College, Mumbai, India.
*Corresponding author E-mail: shravaniwadekar996@gmail.com

http://dx.doi.org/10.13005/ojc/410209

(Received: February 07, 2025; Accepted: March 15, 2025)

ABSTRACT

This study explores the green synthesis, characterization, and cytotoxicity of zinc oxide nanoparticles (ZnO NPs) derived from *Cassia fistula* leaves extract. The biosynthesized ZnO NPs were characterized using UV-Vis spectroscopy, FTIR, PXRD, FESEM, HRTEM, and EDAX analysis. UV-Vis and FTIR confirmed the formation of ZnO NPs and the presence of functional groups involved in the synthesis. PXRD analysis determined the average crystalline size to be 14.91 nm, while FESEM and HRTEM revealed a hexagonal wurtzite structure with irregular morphology. EDAX confirmed a zinc content of 70.5%. The cytotoxicity of ZnO NPs was evaluated on a non-cancerous fibroblast cell line (NIH-3T3) using the MTT assay, demonstrating an IC_{50} value of 38.56 µg/mL. ZnO NPs has higher cytotoxicity and lower cell viability than commercial ZnO sample, even at low concentrations. Thus, this study highlights ZnO NPs to be sustainable and cost-effective biomedical alternative, warranting additional research into their anticancer and antibacterial properties.

Keywords: *Cassia Fistula*, ZnO NPs, Fibroblast cell line, MTT assay, Cytotoxicity effect.

INTRODUCTION

Biomedical research has shown a great deal of interest in ZnO NPs due to their unique physicochemical characteristics, such as a high surface area, particular crystal structure, improved surface-volume ratio, and exceptional antibacterial and antioxidant activities. Biomedical applications, especially in wound healing, acknowledge ZnO NPs for their antimicrobial characteristics, biocompatibility, and ability to promote cell proliferation and migration. Conventional techniques for synthesizing ZnO NPs frequently involve toxic chemicals and demand substantial energy consumption. This poses environmental risks and limits their use in medical applications. To address these challenges, green

synthesis offers a considerable approach that utilizes biological resources like plant extracts to create a sustainable and environmentally friendly alternative. Plant-mediated synthesis employs phytochemicals found in natural extracts, such as phenolic acids, flavonoids, tannins, etc., which function as reducing, capping, and stabilizing agents. As a result, nanoparticles of specified size and morphology are produced without the need for supplementary synthetic chemicals.

Cassia fistula, also referred to as Bahava, Golden Shower, or Amaltas, plays a crucial role in the synthesis of ZnO NPs is attributed to the higher levels of flavonoids and phenolic acids, phytochemicals recognized for their antioxidant, anti-inflammatory, and other advantageous properties, essential for the conversion of metals into metal oxide nanoparticles. Furthermore, the accessibility and cost-effectiveness of bahava leaves render them a feasible choice for synthesizing ZnO NPs with enhanced dimensions and morphology[1-3].

This study highlights the effect of biosynthesized ZnO NPs derived from plant-based methods, on fibroblast cell lines using MTT assay as a potential and multifaceted method for improving wound care treatments. The 3-(4,5-dimethylthiazol-2-yl)-2,5-diphenyltetrazolium bromide assay, or MTT assay, is a traditional colorimetric technique used to measure cellular metabolic activity, hence serving as an indirect measure of cell viability and proliferation. The MTT assay is a prevalent technique for evaluating cell viability and cytotoxicity in diverse biological and pharmacological research. This assay relies on the capacity of metabolically active cells to convert the yellow tetrazolium dye (MTT), into insoluble purple formazan crystals by the action of mitochondrial dehydrogenases. The total amount of formazan generated is directly correlated with the number of live cells and can be measured using a spectrophotometer to measure absorbance at 570 nm after the crystals have been dissolved. The MTT assay technique is straightforward, dependable, and extensively utilized for assessing cell proliferation, medication screening, and toxicological investigations[4-6].

The combination of therapeutic effectiveness, safety, and ecological sustainability renders them a favoured choice for modern wound care treatments. The synthesis of ZnO NPs with phytochemical elements from *Cassia fistula* plant leaves has demonstrated a more adaptable, cost-effective, practical, and eco-friendly approach to enhance the natural processes of wound healing and tissue regeneration.[7-10]

The biological potential of *Cassia fistula*-derived ZnO NPs presents numerous exciting future research opportunities. Additionally, *in-vitro* and *in-vivo* investigations are required to confirm their biocompatibility, toxicity, and therapeutic efficacy in cancer treatment and drug delivery. Investigating mechanistic processes, including their involvement in ROS production, apoptosis, and cellular interactions, may improve their utilization in targeted cancer therapy. Moreover, surface changes and nanocomposite formulations can enhance stability, selectivity, and regulated drug release. Therefore, enhancing their application in antimicrobial coatings, wound healing, and biosensing technologies will solidify their significance in nano-medicinal field.[11-14] Future research should concentrate on integrating ZnO NPs with other nanoparticles forming hybrid by establishing standardized, effective, and safe treatments to be incorporated into conventional medical practice, offering a novel approach for managing complex and chronic wounds, particularly diabetic wounds, as well as creating infection-sensitive bandages specifically for diabetic and burn injuries.[15-18]

MATERIALS AND METHODS

The Mancherji Joshi Five garden at the Central Railway Colony in Mumbai, Maharashtra, was the source of the Cassia fistula plant leaves. The weather conditions reported were 29°C temperature with 71% humidity.

After letting the plant twig air dry for ten to twelve days, it was prepared into an herbarium specimen and authenticated at Blatter Herbarium (BLAT) in St. Xavier's College, Mumbai, to certify the species. The leaves were first removed from the twig and rinsed with tap water and distilled water twice to remove any dust particles. They were then ground into a fine powder and sieved through a size 60 mesh. The powdered leaf sample was securely packaged in an airtight glass jar for future use.

All chemicals were of A.R. grade with 100 percent purity. Zinc Nitrate Hexahydrate, Sodium Hydroxide pellets, double distilled water, distilled water, acetone, and ethanol were obtained from LOBA CHEMIE (Laboratory Reagent and Fine Chemicals), Mumbai, India, of 98 percent purity with CAS number 10196-18-6.

Supplementary reagents for the MTT assay comprise of MTT reagent, dimethyl sulfoxide, formazan crystals and acetic acid all of A.R. grade from SD Fine-Chem Ltd. (SDFCL). Sterile conditions under laminar flow were maintained and pure distilled water was utilized throughout the course of the study.

The mouse fibroblast cell line (NIH 3T3) was obtained from the National Fungal Culture Collection of India (NFCCI) at the Agharkar Research Institute in Pune and utilized for the MTT experiment. Cells were reactivated and subsequently inoculated into a 96-well plate under extremely sterile conditions. Positive control (cells treated with known sample) and negative control (untreated cells) were used to study comparative experimental results. Also, a triplet study was carried out to enhance reproducibility and self-assurance with the results.

Synthesis of ZnO NPs

The extract of bahava leaves was made using an ultrasonic processor (Phoenix Ultrasonic Cleanser PH-UC-120, 100 W, 40 kHz). Leaves were dried and processed into a fine powder. 10 g of finely powdered leaves were mixed with 100 mL of pure distilled water in an Erlenmeyer flask, covered with aluminium foil, and subjected to ultrasonic treatment for two hours at 100°C, the boiling point of water, to ensure complete extraction of phytochemicals from the plant material. Whatman filter paper number 41 was used to filter the mixture in order to extract the residue. 50 mL of the filtrate was combined with 5 g of Zinc Nitrate Hexahydrate ($Zn(NO_3)_2 \bullet 6H_2O$) crystals and stirred on a magnetic stirrer for one hour at 60°C to guarantee comprehensive mixing. The flask is placed in the ultra-sonicator, and a 1M sodium hydroxide (NaOH) solution is added to maintain alkaline conditions to establish pH 11. The mixture is subjected to ultrasonication for an additional two hours to ensure the complete precipitation of ZnO NPs. Upon completion of precipitation, the mixture is then filtered using Whatman filter paper no. 41. Double-distilled water is employed to wash the precipitate three times, followed by ethanol, to guarantee the thorough elimination of contaminants. The residue is then dried in a microwave oven at 60°C for two hours to remove any moisture. The resultant yellow product is zinc hydroxide ($Zn(OH)_2$), which is converted into ZnO NPs via calcination in a muffle furnace for two hours at 500°C. The ultimate product is white ZnO NPs (Figure 1).

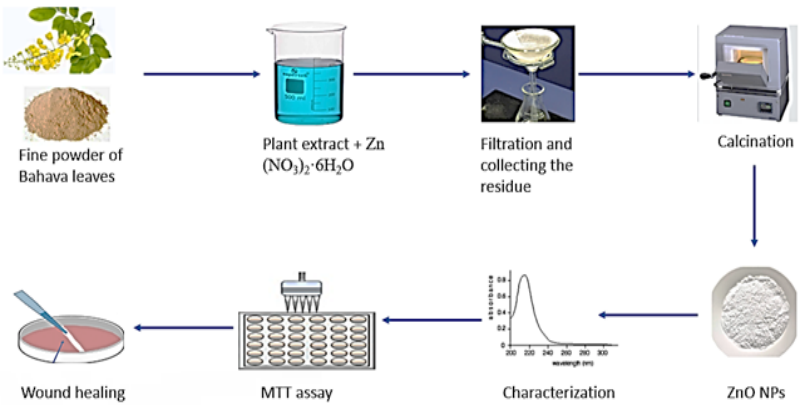

Fig. 1. Schematic representation for biosynthesis of ZnO NPs used for MTT assay

MTT Assay: Test Cell line- NIH 3T3 (Fibroblast Cells)

***In-vivo* cytotoxicity study:** ZnO NPs and commercial ZnO were further diluted to form a working concentration of 0.001 mg/mL, 0.01 mg/mL, and 0.1 mg/mL respectively. The stock solution provided was 0.1g in 10 mL equivalent to 10mg/mL for both ZnO NPs and commercial samples. The samples were sonicated for 2 h before being added to the cells for the experiment.

Protocol: A 96-well plate was seeded with 0.05 million NIH 3T3 cells following cell rejuvenation. During the overnight incubation period,

the cells were maintained at 37°C with 5% CO_2. Following a microscope-based confirmation of cell confluency, the cells were exposed at seven different concentrations. The cells were cultured overnight at 37°C with 5% CO_2 in a CO_2 incubator. The cells were subsequently examined under a microscope for four hours following the addition of 10 µL of 5 mg/mL MTT reagent to each well. After the medium was discarded, 100 µL of DMSO was added to dissolve the formazan crystals.

A 570 nm measurement of the absorbance was measured using microplate reader (Figure 2).

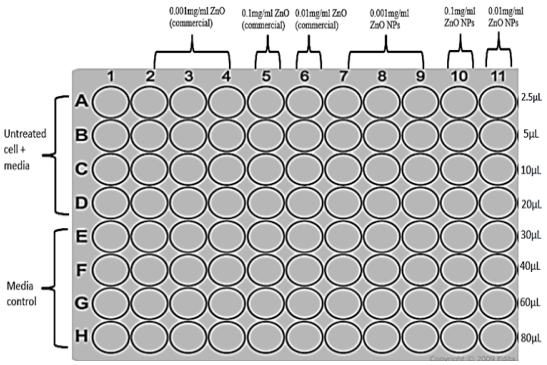

Fig. 2. Diagrammatic illustration of the MTT assay procedure

RESULTS

Characterization of biosynthesized ZnO NPs through various analytical Techniques are listed below:

Ultraviolet-Visible Spectroscopy (UV-Vis):

UV-Vis spectroscopy facilitates the analysis of optical properties to verify the synthesis of ZnO NPs. A prominent peak at 364 nm (Fig. 3) indicates a range nearer to the threshold value of 368 nm, justifying that ZnO NPs may still absorb this light to form electron-hole pairs for diverse applications, including photodetectors and photocatalysis.

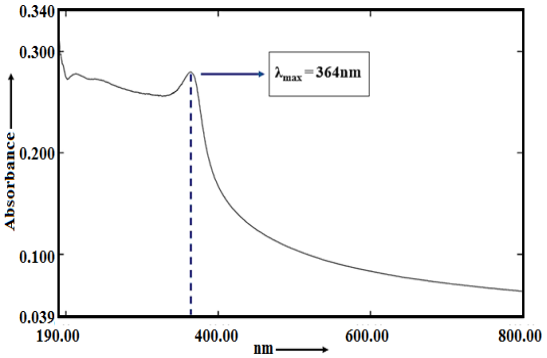

Fig. 3. UV-Vis spectrum of ZnO NPs at 364nm

Fourier Transmission Infrared Spectroscopy:

FTIR facilitates the identification of predominant functional groups in various plant phytoconstituents, contributing to the reduction, stability, and production of nanoparticles. A broad band at 3527.80 cm^{-1} indicates presence of the hydroxy or water molecule adsorbed on the ZnO NPs surface. A peak at 2341 cm^{-1} indicates the potential for CO_2 adsorption, a phenomenon frequently observed in ZnO NPs exposed to atmospheric conditions. This may influence the surface characteristics and reactivity of ZnO NPs in various applications. A peak at 1535 cm^{-1} signifies N-H bending vibrations, primarily originating from amine or amide groups on the surface of ZnO nanoparticles, maybe due to the use of zinc nitrate in the synthesis process. The signal at 1421.54 cm^{-1} indicates surface change mostly resulting from the use of capping agents. An intense absorption band for Zn-O stretching vibration is observed at approximately between 500–600 cm^{-1}. A peak at 501.49 cm^{-1} and 516.92 cm^{-1} proves the presence of the Zn-O stretching and signify metal-oxygen bond (Figure 4).

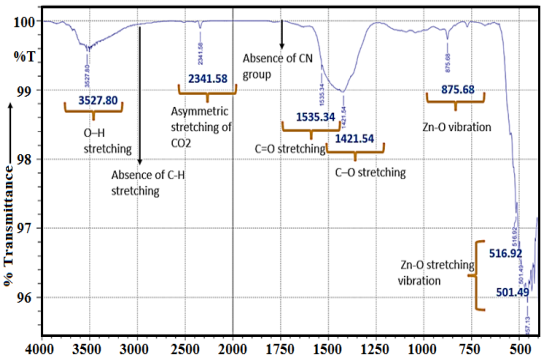

Fig. 4. FTIR analysis of ZnO NPs

Powder X-Ray Diffraction

Powder X-Ray Diffraction of ZnO NPs was analysed using 30mA current and 46KV of voltage and was recorded on carbon-potash radiation (CPR) and scanned at 2θ. The PXRD analysis reveals prominent peaks at (31.7°), (34.4°), (36.2°), (47.5°), (56.6°), (62.8°), (67.9°), and (69.5°), corresponding to the (100), (002), (101), (102), (110), (103), (112), and (201) planes, along with corresponding Full Width at Half Maximum (FWHM) values. These results correspond with the Joint Committee on Powder Diffraction Standards (JCPDS), validating that the ZnO NPs display a hexagonal Wurtzite structure. The average crystalline size of 14.91 nm was calculated utilizing the Debye-Scherrer equation ($D = k\lambda/\beta\cos\theta$) and matched with conventional values. The peaks sharpness suggested the sample's high crystallinity (Figure 5).

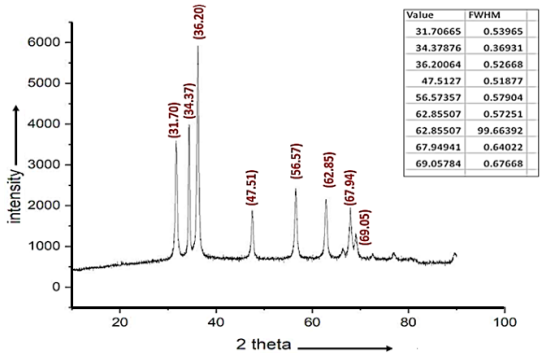

Fig. 5. PXRD analysis of ZnO NPS having the crystalline size of 14.91nm

Field Emission Scanning Electron Microscope

Analysis was done by dispersing ZnO NPs on a carbon-coated grid. FESEM examination reveals that ZnO NPs exhibit a hexagonal-wurtzite morphology. The different-magnification images (a), (b), (c) and (d) provided by this technique facilitate the analysis of surface morphology, shape, and particle size of the nanoparticles, Images (a) and (b), featuring a scale bar of 200 nm, depict highly crystalline nanoparticles exhibiting a hexagonal wurtzite structure, whereas images (c) and (d), with a scale bar of 1 µm, illustrate aggregation or less ordered nanoparticles. Consequently, FESEM elucidates surface properties, including the presence of hexagonal or irregular patterns, as well as aggregation (Figure 6).

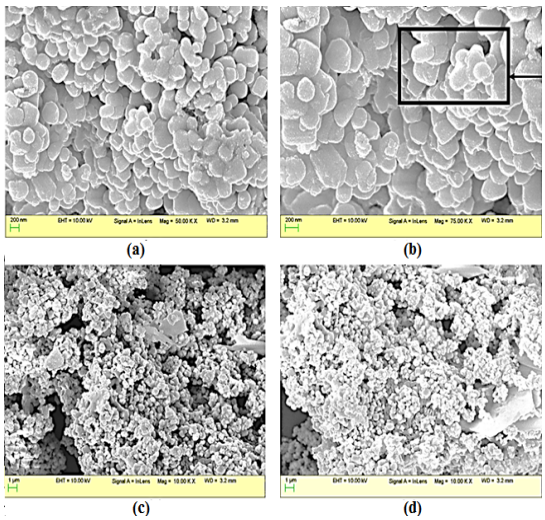

Fig. 6. FESEM analysis of ZnO NPs showing hexagonal-wurtzite structure along with their agglomerates

High-Resolution Transmission Electron Microscopy

ZnO NPs were distributed in deionized water and were placed on a carbon-coated grid, and later dried and evaluated.

HR-TEM explains the structural and particle size distribution of the ZnO NPs. The high-resolution magnified images of ZnO NPs having irregular, spherical, and hexagonal morphology can be inferred from the HRTEM results. The particle distribution was computed following the digitization of the different HRTEM images, and the outcomes were discovered to be consistent with the XRD investigation (Figure 7).

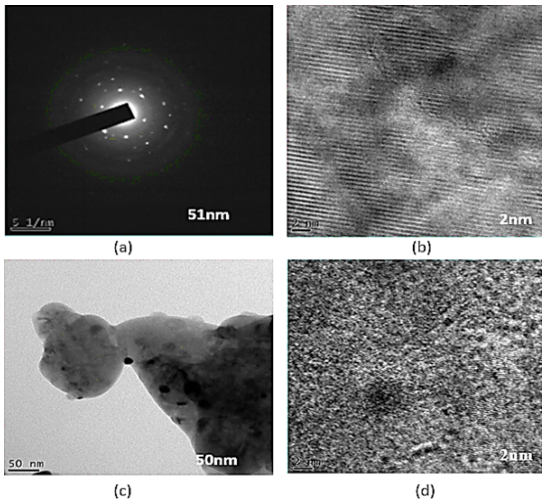

Fig. 7. High-Resolution HRTEM examination of ZnO NPs

Energy Dispersive X-Ray Analysis

EDAX quantifies the zinc element percentage present in the ZnO NPs sample. The significant X-ray emission peak corresponds with the sample's elemental composition, indicating that zinc constitutes 70.5% followed by oxygen at 29.5%. The increased zinc percentage content corresponds with the ZnO NPs sample, thus confirming its presence with a sharp peak intensity confirming its high pure crystallinity (Figure 8).

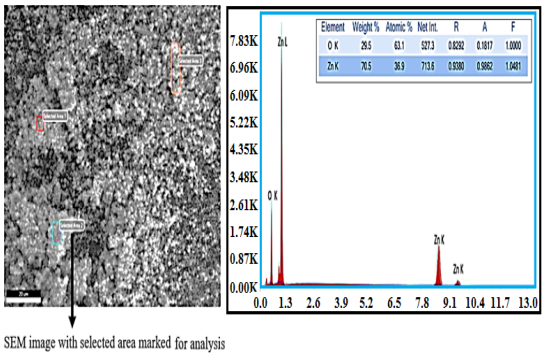

Fig. 8. EDAX analysis of ZnO NPs with percentage elemental composition of zinc and oxygen

In-vitro cytotoxicity study: MTT assay

Figure 9 indicates MTT assay results for commercial ZnO, ZnO NPs and controlled samples.

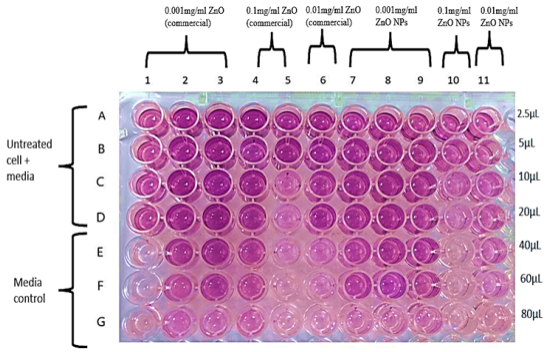

Fig. 9. MTT assay results for commercial ZnO and ZnO NPs samples of varying concentration

Concentrations of samples added for MTT assay

MTT assay for test samples in varying concentrations ranging from 2.5 µL to 80 µL, as shown in Fig. 9. Lane 1: A-D: Untreated cells, E-G: Media control, Lane 2, 3 & 4: 0.001mg/mL commercial ZnO (triplets), Lane 5: 0.1mg/mL commercial ZnO, Lane 6: 0.01mg/mL commercial ZnO, Lane 7, 8 & 9: 0.001 mg/mL ZnO NPs (triplets), Lane 10: 0.1 mg/mL ZnO NPs, Lane 11: 0.01 mg/mL ZnO NPs. The IC_{50} value for each sample can be calculated using the following formula,

Percent Cytotoxicity = Absorbance of control (untreated cells)/Absorbance of treated sample × 100; Percent Cytotoxicity = 100 – Percent Viability.

Table 1: Comparative analysis of MTT assay utilizing 0.001mg/ml of ZnO Commercial sample

Volume of sample (µL)	Concentration µg/mL	Average OD	%Viability	%Cytotoxicity	Mean IC_{50}
2.5	5	0.826	86.180	13.820	
5	10	0.806	84.060	15.940	
10	20	0.798	83.226	16.774	
20	40	0.747	77.942	22.058	54.38 µg/mL
40	80	0.646	67.341	32.659	
60	120	0.549	57.261	42.739	
80	160	0.450	46.903	53.097	

Table 2: Comparative analysis of MTT assay utilizing 0.01 mg/mL of ZnO Commercial sample

Volume of sample (µL)	Concentration µg/mL	Average OD	%Viability	%Cytotoxicity	Mean IC_{50}
2.5	5	0.725	75.579	24.421	
5	10	0.635	66.194	33.806	
10	20	0.134	13.952	86.048	
20	40	0.029	3.003	96.997	14.09 µg/mL
40	80	0.039	4.046	95.954	
60	120	0.017	1.794	98.206	
80	160	0.012	1.199	98.801	

Table 3: Comparative analysis of MTT assay utilizing 0.1 mg/mL of ZnO Commercial sample

Volume of sample (µL)	Concentration µg/mL	Average OD	%Viability	%Cytotoxicity	Mean IC_{50}
2.5	5	0.826	86.180	13.820	54.38 µg/mL
5	10	0.806	84.060	15.940	
10	20	0.798	83.226	16.774	
20	40	0.747	77.942	22.058	
40	80	0.646	67.341	32.659	
60	120	0.549	57.261	42.739	
80	160	0.450	46.903	53.097	

Table 4: Comparative analysis of MTT assay utilizing 0.001 mg/mL of ZnO NPs sample

Volume of sample (µL)	Concentration µg/mL	Average OD	%Viability	%Cytotoxicity	Mean IC_{50}
2.5	5	0.882	92.019	7.981	38.56 µg/mL
5	10	0.863	90.003	9.997	
10	20	0.807	84.164	15.836	
20	40	0.744	77.629	22.371	
40	80	0.680	70.956	29.044	
60	120	0.594	61.988	38.012	
80	160	0.512	53.403	97.001	

Table 5: Comparative analysis of MTT assay utilizing 0.01 mg/mL of ZnO NPs sample

Volume of sample (µL)	Concentration µg/mL	Average OD	%Viability	%Cytotoxicity	Mean IC_{50}
2.5	5	24.213	82.044	17.956	33.30 µg/mL
5	10	26.715a	76.621	23.379	
10	20	34.223	70.469	29.531	
20	40	49.030	64.943	35.057	
40	80	96.684	63.170	36.830	
60	120	98.665	48.571	51.429	
80	160	99.187	21.147	78.853	

Table 6: Comparative analysis of MTT assay utilizing 0.1 mg/mL of ZnO NPs sample

Volume of sample (µL)	Concentration µg/mL	Average OD	%Viability	%Cytotoxicity	Mean IC_{50}
2.5	5	0.727	75.787	24.213	34.33 µg/mL
5	10	0.703	73.285	26.715	
10	20	0.631	65.777	34.223	
20	40	0.489	50.970	49.030	
40	80	0.032	3.316	96.684	
60	120	0.013	1.335	98.665	
80	160	0.008	0.813	87.002	

The following analysis can be interpreted from Table 1, Table 2, Table 3, Table 4, Table 5 and Table 6.

Comparative evaluation using IC_{50} value

ZnO NPs exhibited an IC_{50} value of 33.30 µg/mL as compared to commercial ZnO sample with IC_{50} value of 14.09 µg/mL at the same concentration of 0.01 mg/mL of the sample, thereby indicating superior efficacy of ZnO NPs in inhibiting fibroblast cell migration against commercial ZnO sample.

Comparative analysis for cytotoxicity

At a minimal dosage of 0.001 mg/mL, the commercial ZnO sample demonstrates cytotoxicity between 13.82% and 53.09% across a volume range of 2.5 µL to 80 µL, whereas ZnO NPs exhibit cytotoxicity from 7.98% to 46.59% within the same volume range. At a medium concentration of 0.01 mg/mL, commercial ZnO sample showed cytotoxicity from 24.42% to 98.80% and 17.95% to 78.85% for ZnO NPs sample. At a dosage of 0.1 mg/mL, the commercial ZnO sample maintain cytotoxicity between 13.82% to 53.09%, while ZnO NPs show significantly higher cytotoxicity range from 24.21% to 87.00%. In all the three cases, cytotoxicity values are inversely related to those of cell viability.

DISCUSSION

ZnO NPs can be produced using *Cassia fistula* plant leaves, and proves to be a pragmatic, sustainable, and eco-friendly process. Bioactive constituents in the extract, including flavonoids and phenolic acids, work as reducing, capping, and stabilizing agents, facilitating the conversion of Zn to ZnO NPs without the need for additional synthetic stabilizers. UV-VIS spectroscopy indicates a prominent spectral peak at 364 nm, confirming the synthesis of ZnO NPs (Fig. 3). Fourier Transform Infrared Spectroscopy (FTIR) shows a characteristic Zn-O stretching peak for ZnO NPs, along with peaks corresponding to functional groups from the leaf extract (Fig. 4). X-ray diffraction (XRD) analysis indicates an average crystalline size of 14.91 nm, Field Emission Scanning Electron Microscopy (FESEM) and High-Resolution Transmission Electron Microscopy (HRTEM) validate the hexagonal-wurtzite structure along with spherical and irregular morphology of the ZnO NPs, which lie within the predicted size range (Fig. 5, Fig. 6 and Fig. 7) respectively. The ZnO NPs purity is further supported by Energy Dispersive X-ray Analysis (EDAX), which shows a prominent peak that indicates high material quality and a zinc content of 70.5% (Fig. 8). ZnO NPs were tested for cytotoxicity on a fibroblast cell line using the MTT cytotoxicity technique. The results show that the ZnO NPs exhibit a maximum cytotoxicity of 87.00% with a concentration of 0.1 mg/mL for a volume of 80 µL, which is higher than the commercial ZnO counterpart, which showed 53.09% cytotoxicity at the same volume and concentration. Also, at the lowest concentration of 0.001 mg/mL, ZnO NPs showed the maximum cytotoxicity of 97.00% at 80 µL as compared to

commercial ZnO sample with maximum cytotoxicity of 53.09% at the same volume and concentration (Fig. 9, Table 1, Table 2, Table 3, Table 4, Table 5, Table 6, Table 7, and Table 8). These results suggest that ZnO NPs, in their nano-formulation, may exhibit maximum cytotoxicity even at the lowest concentrations (0.001 mg/mL) than commercial ZnO sample, likely due to their distinct characteristics including a high surface-area-to-volume ratio and enhanced reactivity. These variables contribute to the interaction of nanoparticles with biological systems, consequently triggering the formation of oxidative stress through the production of increased reactive oxygen species, resulting in cellular disruption and ultimately cell death.[19-20]

Therefore, careful evaluation of nanoparticle formulations and appropriate dosage levels is crucial for further studies and biomedical applications.

All aforementioned results are original and were generated by the author for a study on the biosynthesis of ZnO NPs and their cytotoxicity, conducted in December 2024.

CONCLUSION

This research work successfully demonstrates a sustainable method for synthesizing ZnO NPs from the extract of *Cassia fistula* plant leaves, validated by several advanced analytical techniques such as UV-Vis, FTIR, PXRD, FESEM, HRTEM, and EDAX analysis to check its nano structured size and overall morphology of nanoparticles. The cytotoxicity investigation was performed using the MTT assay on a mouse fibroblast cell line (NIH-3T3), based on varying concentrations of ZnO NPs, and compared with commercial ZnO sample. Biosynthesized ZnO NPs demonstrated superior cytotoxicity and less cell viability compared to commercial ZnO sample, even at the minimal dose of 0.001 mg/mL. Due to the nanoscale dimensions of ZnO NPs and their small surface-to-volume ratio, the generation of reactive oxygen species occurs and results in oxidative stress that causes cellular death. Subsequent research may encompass the examination of ZnO NPs for biomedical applications, including anticancer and antibacterial activities, as well as wound healing. Therefore, a pharmacological investigation with a dose-dependent formulations will be necessary for therapeutic application. Moreover, the release of ZnO NPs and its mechanism with the target site can be controlled by optimizing certain parameters.

ACKNOWLEDGEMENT

The authors express profound gratitude to Dr. P.S. Ramanathan Laboratory at Ramnarain Ruia Autonomous College, ICT (Institute of Chemical Technology) in Matunga, IIT (Indian Institute of Technology) Mumbai, NFB (National Facility for Biopharmaceuticals) at Khalsa College in Matunga, and ICON Labs in Navi Mumbai for their invaluable support in characterization and data analysis.

Conflict of Interest

The authors hereby declare that no conflict of interest exist among themselves.

REFERENCES

1. Ragavendran, C.; Kamaraj, C.; Alrefaei, A. F.; Priyadharsan, A.; De Matos, L. P.; Malafaia, G.; Moulishankar, A., & Thirugnanasambandam, S., *South African Journal of Botany.*, **2024**, *167*, 643–662. https://doi.org/10.1016/j.sajb.2024.02.049
2. Wu, C.; Zhang, T.; Ji, B.; Chou, Y., & Du, X., *Cellulose.*, **2024,** *31*(8), 4849–4864. https://doi.org/10.1007/s10570-024-05914-9
3. Zhou, D.; Ge, M.; Wang, Q.; Sun, J.; Yao, H.; Deng, Y.; Xiao, L.; Wang, J., & Wei, J., *ACS Biomaterials Science & Engineering.*, **2024**, *10*(6), 3883–3895. https://doi.org/10.1021/acsbiomaterials.4c00107
4. Kamarajan, G.; Anburaj, D. B.; Porkalai, V.; Muthuvel, A., & Nedunchezhian, G., *J. of the Indian Chemi. Society.*, **2022**, *99*(10), 100695. https://doi.org/10.1016/j.jics. 2022.100695
5. Vijayakumar, S.; Vaseeharan, B.; Malaikozhundan, B., & Shobiya, M., *Biomedicine & Pharmacotherapy.*, **2016**, *84*, 1213–1222. https://doi.org/10.1016/j.biopha.2016.10.038
6. Astaneh, M. E., & Fereydouni, N., *ACS Omega.*, **2024**, *9*(40), 41107–41129. https://doi.org/10.1021/acsomega.4c04961
7. Dong, Y.; Wang, Z.; Wang, J.; Sun, X.; Yang, X., & Liu, G., *Journal of Biological Engineering.*, **2024**, *18*(1). https://doi.org/10.1186/s13036-023-00402-3.

8. Asif, N.; Amir, M., & Fatma, T., *Bioprocess and Biosystems Engineering.*, **2023**, *46*(10), 1377–1398. https://doi.org/10.1007/s00449-023-02886-1.
9. Khatami, M.; Varma, R. S.; Zafarnia, N.; Yaghoobi, H.; Sarani, M., & Kumar, V. G., *Sustainable Chemistry and Pharmacy.,* **2108**, *10*, 9–15. https://doi.org/10.1016/j.scp.2018.08.001
10. Agila, A.; Dakshayani, R.; Vimala, J. R.; Bharathy, M. S.; Sheela, S. M.; Vimala, S.; & Nivetha, S., *Orient. J. Chem.,* **2024**, *40*(4), 1061–1066. https://doi.org/10.13005/ojc/400417
11. Kumar, M.; Swamy, B. E. K.; Reddy, S.; Kumara, J. K. S., & Zhao, W., *Journal of the Electrochemical Society.*, **2020**, *167*(8), 087511. https://doi.org/10.1149/1945-7111/ab91c9
12. F, F., Thabassoom, H. A., Ruby, S. A., & Florence, J. F., *Orient. J. Chem.,* **2021**, *37*(4), 911–921. https://doi.org/10.13005/ojc/370420
13. Kumar, M.; Swamy, B. K.; Reddy, S.; Zhao, W.; Chetana, S., & Kumar, V. G., *Journal of Electroanalytical Chemistry.,* **2019**, *835*, 96–105. https://doi.org/10.1016/j.jelechem.2019.01.019
14. Kumar, M., Swamy, B. E. K., Reddy, S., Sathisha, T. V., & Manjanna., *J. Analytical Methods.*, **2012**, *5*(3), 735–740. https://doi.org/10.1039/c2ay26124c
15. Batool, M.; Khurshid, S.; Qureshi, Z., & Daoush, W. M., *Chemical Papers.*, **2020**, *75*(3), 893–907. https://doi.org/10.1007/s11696-020-01343-7
16. Shabbir, M. A.; Naveed, M.; Rehman, S. U., Ain, N. U., Aziz, T., Alharbi, M., Alsahammari, A., & Alasmari, A. F., *ACS Omega.*, **2023**, *8*(37), 33358–33366. https://doi.org/10.1021/acsomega.3c02744
17. Sudhakar, C.; Poonkothai, M.; Selvankumar, T., & Selvam, K., *Journal of Materials Science Materials in Electronics.*, **2022**, *33*(14), 11434–11445. https://doi.org/10.1007/s10854-022-08116-w
18. Grela, E.; Kozłowska, J., & Grabowiecka., *Acta Histochemica.*, **2018**, *120*(4), 303–311. https://doi.org/10.1016/j.acthis.2018.03.007
19. Jayachandran, A., TR, A., & Nair, A. S., *Biochemistry and Biophysics Reports.*, **2021**, *26*, 100995. https://doi.org/10.1016/j.bbrep.2021.100995
20. Lin, C.; Lee, M.; Chi, M.; Chen, C., & Lin, H., *ACS Omega.*, **2019**, *4*(1), 1801–1809. https://doi.org/10.1021/acsomega.8b02321 d